A Treatment Outcome Prediction Model of Visual Field Recovery Using Self-Organizing Maps

Tobias Guenther*, Iris Mueller, Markus Preuss, Rudolf Kruse, *Fellow, IEEE*, and Bernhard A. Sabel

***Abstract*—Brain injuries caused by stroke, trauma, or tumor often affect the visual system that leads to perceptual deficits. After intense visual stimulation of the damaged visual field or its border region, recovery may be achieved in some sectors of the visual field, but the extent of restoration is highly variable between patients and is not homogeneously distributed in the visual field. We now assess the visual field loss and its dynamics by perimetry, a standard diagnostic procedure in medicine, to measure the detectability of visual stimuli in the visual field. Subsequently, a treatment outcome prediction model (TOPM) has been developed, using features that were extracted from the baseline perimetric charts. The features in the TOPM were either empirically associated with treatment outcomes or were based on findings in the vision-restoration literature. Among other classifiers, the self-organizing map (SOM) was selected because it implicitly supports data exploration. Using a data pool of 52 patients with visual field defects, the TOPM was constructed to predict areas of improvement in the visual field topography. To evaluate the predictive validity of the TOPM, we propose a method to calculate the receiver operating characteristic graph, whereby the SOM is used in combination with a nearest neighbor classifier. We discuss issues relevant for medical TOPMs, such as appropriateness to the patient sample, clinical relevance, and incorporation of *a priori* knowledge.**

***Index Terms*—Hemianopia, intraindividual prediction, self-organizing map (SOM), treatment outcome prediction model (TOPM).**

I. Introduction

BEING able to predict treatment outcome is important to optimize therapy in modern medicine. To achieve this goal, computerized technology, employing *a priori* knowledge of the disease, is used to help predict specific treatment outcomes. The ability to predict treatment outcomes is not only useful for gaining further insight into mechanisms of recovery (i.e., contributing factors to recovery), but will also aid the clinician in estimating treatment efficacy in individual patients and may provide new insights toward improving effectiveness. We have developed and tested a prediction model in the field of visual system plasticity using self-organizing maps (SOMs) as the core of a treatment outcome prediction model (TOPM). Besides the generally accepted recommendation to favor simple algorithms rather than complex algorithms [1], there is no consensus in the literature as to which algorithm is best suited for a specific problem. We have chosen the SOM because it provides data visualization and can be extended to classification and prediction purposes as well.

Here, the SOM is applied to data obtained from patients with visual field defects caused by stroke, traumatic brain injury, or other etiologies that lead to cerebral lesions. It was observed that such visual field defects can be reduced by systematically presenting visual stimuli at the border region of the damaged visual field [2]–[5] using "vision restoration training" (VRT). Because not all patients can be treated in all areas of the visual field, it is desirable to find methods that efficiently predict the extent of visual restoration. The proposed methods of outcome prediction presented here have potential utility for other medical problems in which topographic diagnostic charts are used. Within this context, we present a TOPM that allows both the prediction of the extent as well as the topographic distribution of the recovery of visual functions in individual patients.

A. Visual System

To enhance the features that are used in the TOPM, we briefly consider some fundamental aspects of the visual system. The visual system information pathway begins at the retina where light is transformed to electrophysiological signals that are transmitted by the retinal ganglion cells through the optic nerve to different brain regions. The primary visual cortex (also called "V1") computes basic features of visual images and scenes and works in concert with many "higher" brain regions to which it is reciprocally connected [6]. The visual system is the largest sensory processing system in the brain. About 30%–50% of the cerebral cortex is committed to process visual information that compares to only 8% in the auditory and 7% in the somatosensory system [7]. This is the reason why brain damage due to stroke or head injury is often accompanied by loss of visual functions as expressed by partial or total blindness. The loss of visual function, as well as its restoration (recovery), is typically assessed by "perimetry," which is a behavioral-/computer-based test, whereby patients are asked to respond to small target stimuli that are presented in a random fashion within the visual field. Depending on the performance of the patients (responding or not responding to the stimulus by pressing a button), diagnostic charts are obtained that describe the location of areas of relative or total blindness (see Fig. 1).

Manuscript received November 9, 2007; revised February 27, 2008, June 6, 2008, August 6, 2008, and October 24, 2008. First published December 9, 2008; current version published April 15, 2009. *Asterisk indicates corresponding author*.

*T. Guenther was with the Institute of Medical Psychology, Otto-von-Guericke University, Magdeburg 39120, Germany. He is now with Elaspix UG, Mannheim 68163, Germany (e-mail: tobias.guenther@med.ovgu.de).

I. Mueller and B. A. Sabel are with the Institute of Medical Psychology, Otto-von-Guericke University, Magdeburg 39120, Germany (e-mail: iris.mueller@med.ovgu.de; bernhard.sabel@med.ovgu.de).

M. Preuss was with the Institute of Medical Psychology, Otto-von-Guericke University, Magdeburg 39120, Germany. He is now with the Institute of Preventive Medicine, University of Rostock, Rostock 18055, Germany (e-mail: markus.preuss@uni-rostock.de).

R. Kruse is with the Department for Knowledge and Language Engineering, Otto-von-Guericke-University, Magdeburg 39104, Germany (e-mail: kruse@iws.cs.uni-magdeburg.de).

Digital Object Identifier 10.1109/TBME.2008.2009995

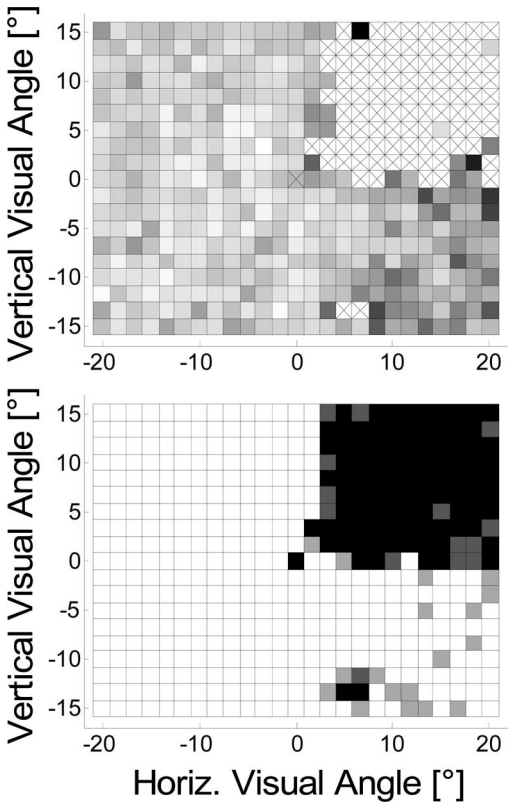

Fig. 1. Visual field diagnostic charts (HRP charts) obtained from computer-based visual field assessments. In each respective location of the chart, three above-threshold stimuli are presented at random time intervals and locations. The top panel displays "reaction time charts" (averaged among the three test stimuli per position). Minimal response time is coded in white (about 350 ms) and maximal response time in black (about 900 ms). Detection misses (no responses) are represented by a cross. Bottom panel: the "detection chart" shows areas with: 1) complete blindness in black (zero out of three stimuli were acknowledged by the subject; chart value: 0); 2) intact vision shown in white (3/3 acknowledged test stimuli; chart value: 1); and 3) areas of residual vision shown in gray (1/3 or 2/3 stimulus presentations were acknowledged, chart value: 1/3, 2/3). This chart is taken from a patient suffering from a quadrantanopia. The diagnostics chart resolution is GX $= 25 \times$ GY $= 19$ stimuli (background luminance: 86 cd/m^2, stimulus luminance: 23 cd/m^2, stimulus size: 0.4°, interstimulus distance: 1.7°). To reduce eye movements that can compromise diagnostic quality, patients are required to fixate on a central fixation point and respond to color changes (catch trials) presented at random intervals.

B. Diagnosis of Damage to Visual System

Diagnostic visual field charts (see Fig. 1) are an important part of neurological and ophthalmologic examination [8]. Visual field testing can detect and localize defective areas as well as monitor dynamic changes (deterioration or recovery) within the visual field [9]. The size, form, and location of a given visual field defect (also called scotoma) are often indicative of the specific location of the damage within the visual pathway. The "high-resolution perimetry" (HRP) assesses the visual field in high spatial resolution with bright, high-contrast (superthreshold) stimuli. The stimuli are presented on a computer screen, which is positioned 40 cm in front of the subject, while the head of the subject is stabilized by using a chin rest (this reduces body and head movements during the diagnostic session). The subject responds by pressing a button whenever the presented test stimuli are perceived. During the diagnostic procedure, the subject fixates on a static point at the center of the diagnostic area (the fixation spot). The diagnostic output is a topographical chart that schematically illustrates the visual field defects of each patient. Several (here, three) single diagnostic tests, which are assessed shortly after each other, are superimposed to obtain a chart that displays visual detections ($\mathrm{Map}_{\mathrm{Detection}}$) and reaction times ($\mathrm{Map}_{\mathrm{ReactionTime}}$). This computer-based perimetric procedure [10] examines the central visual field ($\pm 20°$) in a valid and reliable way [11]. On the basis of these detection charts, three different types of diagnostic spots are defined depending on their state of functionality: 1) total defect with zero detections out of three presentations [denoted with "0" in (1)]; 2) intact vision where patients responded three times correctly after three stimulus detections [denoted with "1" in (2)]; or 3) residual vision with one or two detections [denoted with "1/3" and "2/3" in (3)]. These three diagnostic spot types are defined by the concept of a stencil

$$\mathrm{stencil}_{\mathrm{Defect}}(x,y) = \begin{cases} 1, & \text{iff } \mathrm{map}^{\mathrm{Baseline}}_{\mathrm{Detection}}(x,y) = 0 \\ 0, & \text{else} \end{cases} \quad (1)$$

$$\mathrm{stencil}_{\mathrm{Intact}}(x,y) = \begin{cases} 1, & \text{iff } \mathrm{map}^{\mathrm{Baseline}}_{\mathrm{Detection}}(x,y) = 1 \\ 0, & \text{else} \end{cases} \quad (2)$$

$$\mathrm{stencil}_{\mathrm{Residual}}(x,y) = \begin{cases} 1, & \text{iff } \mathrm{map}^{\mathrm{Baseline}}_{\mathrm{Detection}}(x,y) = \frac{1}{3} \vee \frac{2}{3} \\ 0, & \text{else} \end{cases}. \quad (3)$$

C. Vision Restoration Training

Although the greatest plasticity of the visual system can be found during the postnatal state, it can also be seen in adulthood, within weeks or months following damage to the visual system. Immediately after visual cortex damage (e.g., due to stroke), spontaneous recovery can be observed, putatively mediated by cortical reorganization [12]–[14]. VRT was developed to treat patients after their spontaneous recovery has been completed by visually stimulating the visual field border in order to repetitively activate partially damaged regions located between areas of the intact and defective visual field [2]. The treatment area is adjusted monthly depending on the progress of the patient. When patients with visual field defect carry out this treatment, 1 h per day for a period of six months, significant improvements (enlargements) of the visual field have been observed in 30%–70% of all patients [2]–[5], [15], [16]. The goal of the present study was to develop and test a new outcome prediction model in which extent and the topographic location of visual field restoration can be estimated.

D. Treatment Outcome Prediction

The following is a useful definition of medical prognosis [17]: "Medical prognosis is the prediction of the future course and outcome of disease processes, which may either concern their natural course or their outcome after treatment." In contrast to

predicting the type of a disease, treatment outcome prediction considers the time component [17]. In general, the TOPM is used by clinicians as a recommendation tool to select the treatment with the highest expected benefit to the patient. The prediction model extends the knowledge of the physician and offers the benefit of a second opinion [1]. The TOPM described here predicts the outcome of treating intrasubject visual field areas. The local prediction is "spot-based" (a spot is a point in the visual field) and the treatment outcome of a specific spot is either improvement (termed "hot spot") or no improvement ("cold spot"). Our TOPM methodology comprises the following three steps: 1) building a TOPM that can predict the treatment outcome based on the baseline diagnosis and diagnostic charts from patients who have completed VRT; 2) extracting predetermined features (described later) from a patient's baseline diagnostic charts who has not yet participated in VRT (as either "impaired" spots with zero or one out of three possible detections or "intact" spots with two or three out of three possible detections); and 3) predicting the treatment outcome [based on the features obtained from step 2)] for all impaired spots by using the TOPM [derived in step 1)].

A labeled database was collected to support SOM learning and cross validation, which contains pairs of baseline and post-treatment diagnostic charts from 52 selected patients. Charts from another three patients (not part of the learning set) were chosen randomly to visualize the TOPM output. Diagnostic data were retrospectively selected from a patient pool of two prior studies with hemianopic subjects [4], [18]. Both studies were carried out in accordance with the provisions of the declaration of Helsinki.

II. Feature Selection

Feature selection is the task of deciding which features are relevant to the target classification (in this case, treatment outcome). The suitability of features that are used for the TOPM determines the performance of the prediction model even more than the choice of the classification algorithm [19]. This is important especially within the medical domain where the datasets, when collected automatically, may contain many "don't care" attributes [20]. Hence, features should be evaluated by domain experts using the available numerical information [21]. Accordingly, we selected and constructed appropriate features based on the current practice of VRT and literature of clinical and neuroscientific studies related to VRT. The anatomy of the visual cortex, results of cortical lesion experiments, and the domain knowledge from experts of VRT were considered [10]. To determine the predictive value of the features, several dependent measures, Spearman and Pearson correlation coefficients (ρ), and the analysis of variance (comparing population means μ) were used preceding this study and were tested for statistical significance (p). The examined features were grouped into *global* and *local* features. Global features address chart-related information, while local features relate to a specific spot in the visual chart. A short description of the features and what is known from the literature are given later.

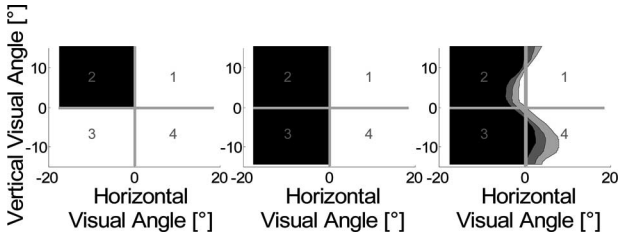

Fig. 2. Prototypic visual field defects. Homonymous quadrantanopia (left) in the upper left quadrant and hemianopia (middle) of the left hemifield. In many patients, the border zone is not as sharp as in the left and middle panels but shows variable performance, i.e., broken up with residual spots forming a diffuse residual border (right).

A. Global Features

1) Size of Residual and Defect Area: The defective sector of the visual field is usually rather compact and covers large areas of the visual field, i.e., up to half of the visual field in patients with hemianopia and about a quarter in quadrantanopia (see Fig. 2). The size of the visual field defect was not significantly correlated with the treatment outcome [16] in contrast to other studies where patients with small defect areas showed a stronger improvement than patients with large defect areas (right eye: $\rho = -0.544$, $p < 0.05$; left eye: $\rho = -0.639$, $p < 0.05$) [23], [24].

Areas of residual vision are usually located at or near the border region that separates the "seeing" field from the "blind" field. But residual vision can also occur in compact areas within the defect or intact visual field. Both features are included in the TOPM and are computed as follows:

$$\text{defect area} = \sum_{y=1}^{GY}\sum_{x=1}^{GX} \text{stencil}_{\text{Defect}}(x,y) \tag{4}$$

$$\text{residual area} = \sum_{y=1}^{GY}\sum_{x=1}^{GX} \text{stencil}_{\text{Residual}}(x,y). \tag{5}$$

It was repeatedly observed that visual field improvements occur in areas where the detection of stimuli is unreliable (termed areas of residual vision indicated by shades of gray in Fig. 1, bottom panel) [5], [15]. Specifically, the size of the residual area before treatment correlated significantly ($\rho = 0.68$, $p = 0.001$) with the treatment outcome [24]–[26]. However, the position of residual spots is somewhat unstable because residual functions are prone to fluctuations caused by fatigue, stimulus saliency, and general attention [27].

2) Reaction Time: The reaction time varies largely between and within subjects. In one study, patients with faster reaction time experienced a more pronounced visual field increase ($\rho = 0.44$, $p < 0.05$) [26], whereas another study (assessing a different group of patients) found no significant correlation between reaction times and treatment outcome [24], [28]. Nevertheless, we considered the reaction time in the TOPM and computed it only from intact spots (such that the reaction time is averaged among three stimulus presentations per location), (6), as shown at the bottom of the next page.

3) Conformity to Hemianopia and Quadrantanopia: This feature expresses the degree of similarity of the visual field of a given patient with a "pure" hemianopia and quadrantanopia, as displayed in Fig. 2. The "pure" hemianopia (one hemifield completely intact and the other hemifield completely blind) is very rare. It may be caused by total anatomical damage of the visual system in one hemisphere. Both features are considered in the TOPM because past clinical experience shows that restoration is unlikely if a visual field defect is complete and close to the pure form [8]. These features are based on combined values from the ratio of defect spots ($\text{ratio}^i_{\text{defect}}$) and the homogeneity ($\text{noise}^i$) of the ith quadrant

$$d^i_{\text{defect}} = \text{ratio}^i_{\text{defect}}(1 - \text{noise}^i). \tag{7}$$

The conformity to hemianopia and quadrantanopia is then calculated from combining the d_{defect} values from all four quadrants [see (8) and (9)] such that, e.g., quadrantanopia of the second quadrant is represented by defect spots in the second quadrant and intact spots in the first, third, and fourth quadrants [see Fig. 2 (left) and (9)]

$$\text{hemianopia} = \max \begin{pmatrix} d^1_{\text{defect}} d^4_{\text{defect}} (1 - d^2_{\text{defect}})(1 - d^3_{\text{defect}}) \\ d^2_{\text{defect}} d^3_{\text{defect}} (1 - d^1_{\text{defect}})(1 - d^4_{\text{defect}}) \end{pmatrix} \tag{8}$$

$$\text{quadrantanopia} = \max \begin{pmatrix} d^1_{\text{defect}} (1 - d^2_{\text{defect}})(1 - d^3_{\text{defect}})(1 - d^4_{\text{defect}}) \\ d^2_{\text{defect}} (1 - d^1_{\text{defect}})(1 - d^3_{\text{defect}})(1 - d^4_{\text{defect}}) \\ d^3_{\text{defect}} (1 - d^2_{\text{defect}})(1 - d^1_{\text{defect}})(1 - d^4_{\text{defect}}) \\ d^4_{\text{defect}} (1 - d^2_{\text{defect}})(1 - d^3_{\text{defect}})(1 - d^1_{\text{defect}}) \end{pmatrix}. \tag{9}$$

4) Border Diffuseness: The extent to which the visual field border is diffuse or sharp is an important parameter that is also typically related to the size of residual vision. Therefore, we have used a "diffuseness" measure by calculating the ratio of residual spots among all spots in the border area (this is described in detail elsewhere [10]). The border area is 5° wide and located between the defect and intact area [see Fig. 3(a)]. The border is defined as "diffuse" if many residual spots lay inside the border area and "sharp" if almost no residual spots are inside the visual scotoma border. In the VRT literature, diffuseness of the border was often proposed as a strong determinant of restoration [4], [5], [15], [29], [30] and is also considered in the TOPM.

B. Local Features

In order to predict the treatment outcome for each spot, local spot-related features are introduced to extend the global features.

1) Distance to Scotoma: The distance between the spot and the scotoma border [see Fig. 3(b)] is estimated in cortical coordinates. By using a coordinate transformation model [31], visual field coordinates are transformed into cortical coordinates considering cortical magnification factor. This feature is utilized in the TOPM as the distance to the scotoma (measured in cortical millimeter) significantly separates ($p < 0.01$) "hot" ($\mu = 3.2 \pm 0.67$ mm) from "cold" spots ($\mu = 5.9 \pm 0.65$ mm) [22].

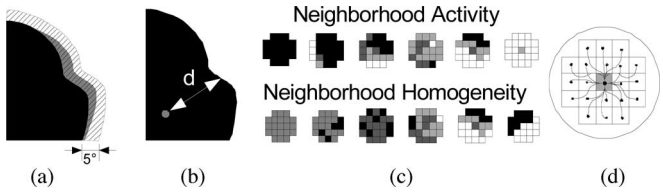

Fig. 3. Schema of global and local features. (a) Global feature *border diffuseness* measures the fraction of residual spots within the border area (hatching), which is defined as the area that touches the defect area and extends 5° into the residual (gray) or intact area (white). (b) *Distance to scotoma* measures the distance d between a spot and the defect border and is estimated in cortical coordinates considering cortical magnification. (c) Schematic illustration representing examples of different local neighborhoods that are differentiated into *neighborhood activity* (top) and *neighborhood homogeneity* (bottom). They are ordered from low to high activity and from high to low homogeneity. (d) Activity and the homogeneity are based on the concept of the local spatial neighborhood, which is inspired by the connectivity between neurons where intrinsic horizontal connections (indicated by branches) exist between neurons.

2) Neighborhood Measures: The probability of restoration is associated with the average activity of spots within a 5° visual angle around a damaged spot [see Fig. 3(c)]. If the surround is relatively intact, and therefore physiologically more active, restoration is more likely. We described elsewhere that the *neighborhood activity* (values between 0 = not active and 1 = fully active) around hot spots ($\mu = 0.37 \pm 0.03$) was significantly ($p < 0.01$) higher than around cold spots ($\mu = 0.10 \pm 0.03$) [22]. Lateral horizontal connections [black branches in Fig. 3(d)] in the visual cortex could explain such a center–surround relationship between neurons in the primary visual cortex. These horizontal connections are anatomically and physiologically well described [46] and their function is to integrate visual information over a specific cortical distance. Another measure to describe the neighborhood is to use measures of variability of the residual activity (*neighborhood homogeneity*) within the immediate surround of the spot, which is the standard deviation from the average of *neighborhood activity*.

3) Visual Field Position: Hot and cold spots are not uniformly distributed in the visual field, but are a function of the location of the visual scotoma, and are therefore considered in the TOPM. It was observed that the eccentricity (which is defined as the distance of the spot from the visual field center in degrees of visual angle) was positively correlated ($\rho = 0.415$, $p < 0.05$) with the amount of the defect border shift (which is comparable to the definition of treatment outcome used in this paper) [24], [28]. In addition, it was hypothesized that recovery follows the cortical magnification, i.e., improvement increases with increasing eccentricity [25].

4) Residual Function: In contrast to *border diffuseness* that measures the amount of residual vision of the whole border, the

$$\text{reaction time} = \frac{\sum_{y=1}^{GY} \sum_{x=1}^{GX} (\text{Map}^{\text{Baseline}}_{\text{Reaction Time}}(x, y) \text{stencil}_{\text{Intact}}(x, y))}{\sum_{y=1}^{GY} \sum_{x=1}^{GX} \text{stencil}_{\text{Intact}}(x, y)} \tag{6}$$

measure *residual function* is directly related to the spot itself and measures the strength of the damage (zero or one detections out of three presented stimuli; spots with two or three detections are not considered because they are not classified as impaired). It is interpreted as the probability of stimulus detection at that particular specific spot position. In a recent study, we found a significantly ($p < 0.01$) higher *residual function* (values between $0 =$ absolute defect and $0.33 =$ residual) of hot spots ($\mu = 0.16 \pm 0.01$) in comparison to cold spots ($\mu = 0.04 \pm 0.01$) [22]. The *residual function* of each spot is equal to the detection chart value at the respective position (x, y)

$$\textit{Residual Function}(x, y) = \left\{ \begin{array}{ll} 0, & \text{iff } \text{map}_{\text{Detection}}^{\text{Baseline}}(x, y) = 0 \\ \dfrac{1}{3}, & \text{iff } \text{map}_{\text{Detection}}^{\text{Baseline}}(x, y) = \dfrac{1}{3} \end{array} \right\}. \quad (10)$$

III. Kohonen Self-Organizing Map

In addition to selecting appropriate features, the development of a TOPM requires selecting an appropriate classification algorithm. SOMs, introduced by Kohonen [32], are based on the calculation of the Euclidean distance in multidimensional space. SOMs have convinced experts of their usability in the medical domain [33]. They are a preferable tool for exploratory data analysis because of their data visualization capabilities; they are used for correlation hunting, unsupervised and supervised cluster analysis, multivariate feature analysis, as well as for novelty detection and classification [34].

A. Data Exploration

In practice, SOMs decompose the high-dimensional feature space into multiple low-dimensional maps (also termed component planes). In this application, the 12-D feature space is substituted by 12 2-D maps. The component planes are feature-specific projections onto the SOM surface after learning. Each plane shows the data distribution separately for the respective feature (see Fig. 4). This operation does not require finding a new interpretation for the resulting components, as would be the case in principal component analysis (PCA; see Fig. 5). The component planes consist of map units that enable the data to be visualized, while preserving the topography of the original feature space. Each map unit has become a highly sensitive feature detector after learning [34]. Importantly, due to the SOM-specific cooperative learning scheme, adjacent map units have similar feature values. The map units represent cluster centers in the data distribution and maintain the same position in each of the 12 component planes, so that, by using location, the distribution of the data samples is visually comparable between the component planes.

The map units are labeled as hot ("+") and cold spots ("0"). The label is not shown for each map unit because the map is separated compactly between hot and cold spot map units. Each data sample in the learning database is assigned to exactly one map unit (minimizing the distance between map unit and data sample). The topography of hot and cold spots in the component planes (see Fig. 4) after learning is relatively robust if the learning process is repeated.

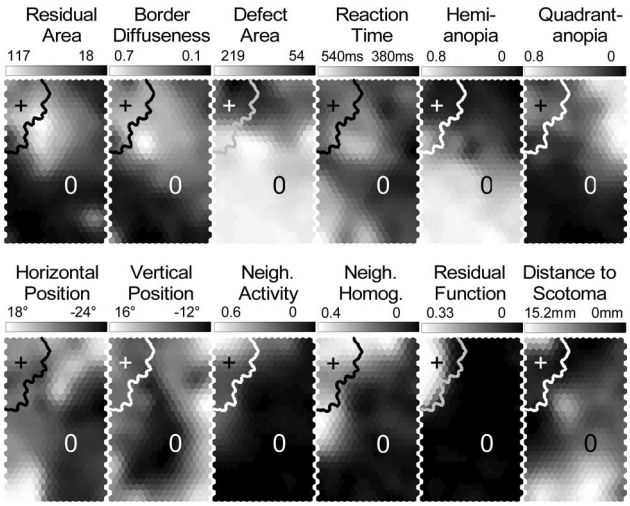

Fig. 4. Component planes of global (top row) and local (bottom row) features extracted from the baseline diagnostic charts. The distribution of values of the respective feature is shown for hot ("+") and cold ("0") spots. These planes are used for both data exploration and prediction.

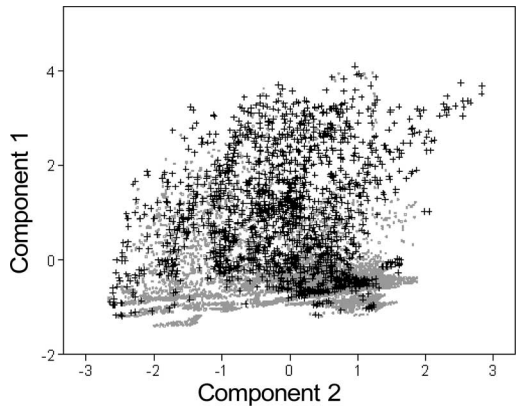

Fig. 5. PCA with varimax rotation (applied to all 12 features, local and global). Four components were determined with an eigenvalue > 1, explaining 69% of the variance. The first two components are shown above. To deduce knowledge from PCA component graphs, an appropriate interpretation of the PCA components must be found. Furthermore, by using only the first two PCA components, a clear discrimination between hot ("+," black) and cold spots ("·," gray) is not visible without adding further PCA components. However, a 3-D (or more) PCA component space reduces the visibility of the data distribution. In contrast, the component charts of the SOM algorithm are 2-D, features specific, and are comparable by location (see Fig. 4).

The distance between the closest cold and hot spot map units in Euclidean space was found to be relatively broad in comparison to the distance between map units belonging to the same class (this was concluded from the distance matrix). This shows, first, that there is a "natural" difference between cold and hot spots in the sample distribution, and second, that a robust discrimination between predicted cold and hot spots exists.

By visual inspection of the component planes, hypotheses about the relationship between the treatment outcome and the various features, as well as their interdependencies, can be formulated. To demonstrate the data exploration by using the

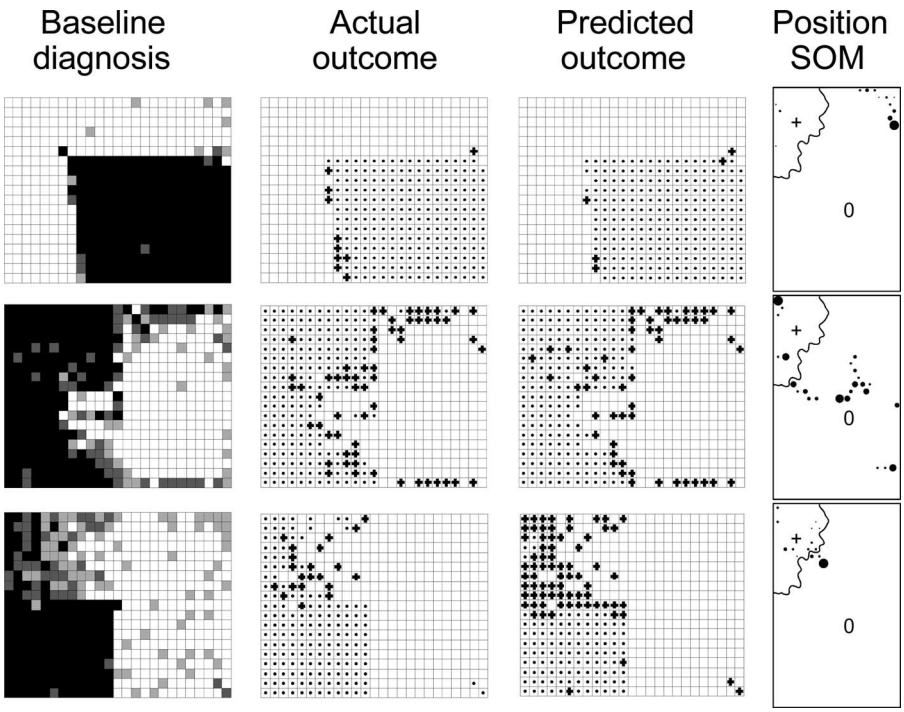

Fig. 6. Diagnostic charts of three randomly selected patients (first column) that were not part of the learning set. The actual treatment outcome is shown in the second column (hot "+" or cold "·" spot). The third column shows the predicted treatment outcome for each impaired spot at baseline. The location of spots from individual baseline charts projected onto the SOM is shown in the right column. The respective SOM location differs widely among the three patients (higher frequencies are indicated by a larger circle size) and reflects the respective values of global and local features.

SOM, we formulated four hypotheses based on the component planes and then evaluated each hypothesis by statistical measures (shown in parentheses).

Hypothesis 1: Little or no restoration (represented by cold spots) is observed in charts with a small *residual area* (values between 18 = few residual spots and 117 = many residual spots, $\mu_{\rm cold} = 41.6, \mu_{\rm hot} = 63.1, p < 0.01$) and with high affinity to *hemianopia* (values between 0 = not compatible with hemianopic pattern and 1 = fully compatible with hemianopic pattern, $\mu_{\rm cold} = 0.51, \mu_{\rm hot} = 0.36, p < 0.01$).

Hypothesis 2: Residual area and *border diffuseness* are strongly positively correlated ($\rho = 0.75$, $p < 0.01$), and *hemianopia* and *quadrantanopia* are strongly negatively correlated ($\rho = -0.78, p < 0.01$), which is indicated by the brightness distribution of the respective features in the component planes.

Hypothesis 3: Residual function is a good discriminator between hot and cold spots; only few map units in the hot spot region have a low value of *residual function* (values between 0 = absolute defect and 0.33 = residual, $\mu_{\rm cold} = 0.02$, $\mu_{\rm hot} = 0.12, p < 0.01$).

Hypothesis 4: The component charts indicate that global features of the visual charts as a whole are less appropriate for prediction than local features. The brightness distribution of the local features (Fig. 4, bottom row) shows a better association with the map unit labeling of hot and cold spots in comparison to the brightness distribution of the global features (Fig. 4, top row). The fourth hypothesis is supported if the features are ranked with respect to the magnitude of each feature's Pearson correlation coefficient with the treatment outcome: *neighborhood activity* ($\rho = 0.49$, local), *neighborhood homogeneity* ($\rho = 0.42$, local), *residual function* ($\rho = 0.38$, local), *residual area* ($\rho = 0.28$, global), *distance to scotoma* ($\rho = -0.24$, local), *defect area* ($\rho = -0.24$, global), *hemianopia* ($\rho = -0.18$, global), *border diffuseness* ($\rho = 0.17$, global), *reaction time* ($\rho = 0.05$, global), *quadrantanopia* ($\rho = 0.04$, global), *horizontal position* ($\rho = 0.03$, local), *vertical position* ($\rho = -0.01$, not significant, local).

B. Treatment Outcome Prediction

After SOM learning, the cluster prototypes (SOM units) can be labeled according to the majority class among the labels of the data samples in the respective cluster. Then, novel data samples can be classified by using k-nearest neighbor (k-NN) classification. The classification depends on the label of the SOM unit with the smallest Euclidean distance to the novel sample. We have chosen k to be equal to 1, as each map unit is a cluster prototype and represents many data samples. Therefore, the "winner takes all" of labeled map units is actually a "majority vote" among labeled samples of the original data distribution. In order to visualize the prediction outcome and make it visually comparable with the actual treatment outcome, both predicted and actual outcomes, which were not part of the learning set, are shown in Fig. 6 for three randomly chosen patients. This involves three steps. First, features were extracted from the baseline charts (see Fig. 6, left column). Second, the location of each spot in the 12-D feature space was located and projected

onto the SOM surface. Third, by using the k-NN algorithm with $k = 1$, the best matching SOM unit was determined for each spot, which determines, thereafter, the predicted class (hot or cold) of the respective spot. The actual treatment outcome [see (11)] as well as the predicted treatment outcome is shown in Fig. 6 (second and third columns)

$$\textit{Actual outcome}(x,y) = \begin{Bmatrix} \text{“hot spot” iff } \text{map}^{\text{Baseline}}_{\text{Detection}}(x,y) \le \frac{1}{3} \wedge \text{map}^{\text{Post}}_{\text{Detection}}(x,y) \ge \frac{2}{3} \\ \text{“cold spot” iff } \text{map}^{\text{Baseline}}_{\text{Detection}}(x,y) \le \frac{1}{3} \wedge \text{map}^{\text{Post}}_{\text{Detection}}(x,y) \ge \frac{1}{3} \end{Bmatrix}. \tag{11}$$

In order to locate the best matching SOM unit for all spots of each individual chart, the projection of all samples in the diagnostic chart onto the SOM surface is shown in Fig. 6 (right column). Almost all samples of the first chart (Fig. 6, top row) are located at the top right position in the SOM. According to the component planes, this area is more strongly related to *quadrantanopia*, with small *residual area* and low *residual function*. Spots of the second diagnostic chart (Fig. 6, middle row) are spread widely on the SOM. The top left corner is related to maximal *neighborhood activity* and the aggregation in the map center is related to negative horizontal coordinates, covering positive and negative vertical coordinates containing low *neighborhood activity*, which adequately describes the defective hemifield on the left. In the third diagnostic chart, the strongest aggregation of spots is located closely to the hot spot border within the region of cold spots (Fig. 6, bottom row). This region is related to negative vertical coordinates with a similarity to both quadrantanopia and hemianopia containing sharp borders. These spots belong to the lower left part of the semiquadrantanopic diagnostic chart, which also has many defects in the upper quadrant of the left hemifield.

C. Model Evaluation

To evaluate the performance of the TOPM, k-fold-cross validation was selected [35]. Cross validation is a resampling method whereby the test dataset is first divided into k disjunctive sets. Instead of calculating only one evaluation measure, k-fold cross validation offers a more robust evaluation [36]. Therefore, the performance measurement procedure is repeated k times using $k-1$ sets (Λ) for SOM learning and the remaining set (Γ) is used as test dataset. The whole patient database is, therefore, used for both learning and evaluation. As a result, the average among all k evaluation measurements is reported. In comparison to other methods, cross validation is an unbiased and robust estimation of the generalization error, but with a higher standard deviation of the obtained measures [37].

With a tenfold cross-validation procedure, ten classifiers were trained and then evaluated with the test samples. We used standard evaluation measures [38] and calculated the average true positive rate (how many hot spots were classified correctly, TPR $= 44\% \pm 4.7\%$) and the false positive rate (how many cold spots were classified as hot spots, FPR $= 6\% \pm 1.9\%$) among all ten classifiers according to

$$\text{TPR} = \frac{\text{TP}}{P}$$
$$\text{FPR} = \frac{\text{FP}}{N} \tag{12}$$

which is based on the number of positive (P, hot spots) and negative samples (N, cold spots) in Γ, as well as the number of correctly classified positive samples (TP) and incorrectly classified negative samples (FP). At first glance, the TPR seems to be insufficient for a clinical application. However, we have shown (see Fig. 6) that our approach can identify regions in the visual field charts with high probability of improvement, even if about 50% of improved spots in these regions are not correctly predicted.

The average accuracy (ACC $= 84.2\% \pm 1.4\%$) measures the amount of correctly classified samples and was found to be slightly better than the average baseline accuracy ($\text{ACC}_{\text{baseline}} = 81\% \pm 1.3\%$), which is the ratio of samples labeled with the most frequent class. Both measures were computed as follows (the former uses the number of correctly classified negative samples, TN):

$$\text{ACC} = \frac{\text{TP} + \text{TN}}{P + N}$$
$$\text{ACC}_{\text{baseline}} = \frac{\max(P,N)}{P+N}. \tag{13}$$

Interestingly, in some “unfortunate” classification problems, the accuracy of established classifiers was even below the baseline accuracy [39], which is acceptable in the case of unequal misclassification costs where the prediction performance of the preferred class is of higher interest than the prediction performance of the nonpreferred class. The small difference between accuracy and baseline accuracy is a result of the strong skewness of the class distribution, because the learning database contained 7026 cold spots, but only 1689 hot spots. This mismatch in the ratio between cold and hot spots is not caused by artifacts, but is a typical event in this field of medicine, because improvement is rare in comparison to nonimprovement.

D. Receiver Operating Curve Analysis

A measure that is robust to skewed class distributions is the receiver operating characteristic (ROC) [36], which is widely used as a standard procedure in performance evaluation of classifiers in the medical domain [40]. A more robust performance measure is achieved if a continuous ROC curve is used, and the area under the ROC curve (AUC $= 0.81$) is computed for the classifier [41]. The curve is obtained by using a probability score that expresses how strongly the sample belongs to the predicted class. For each evaluation step, the scores are then compared with a threshold α increasing from $-\infty$ to $+\infty$. For each discrete value of α, all samples (i in Γ) were labeled with respect to their score and α as follows:

$$\text{label}_i = \begin{Bmatrix} \text{“hot spot” iff } \alpha \ge \text{score}_i \\ \text{“cold spot” iff } \alpha < \text{score}_i \end{Bmatrix} \tag{14}$$

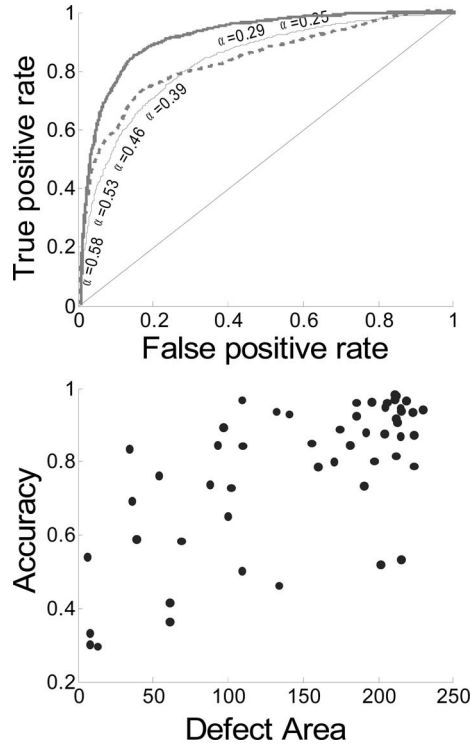

Fig. 7. (Top panel) ROC for the TOPM in prognosis of hot and cold spots in tenfold cross validation. The continuous ROC curve of the TOPM based on the SOM (solid line in black) was calculated by using 1-nearest neighbor classification considering the relative distance to the next hot and cold spot map unit (α, see text). The performance of any classifier that appears around the diagonal is equal to random guessing [36]. For comparison of the SOM performance with alternative methods, the ROC curve was also measured for a SVM (dotted line in gray) and a PCA model (solid line in gray) with four principal components applied to 5-nearest neighbor classification. (Bottom panel) In comparison to tenfold cross validation where the database was divided into ten parts, the spots in the database were divided into 52 parts with respect to patient affiliation. The prediction accuracy was determined for all individual charts in leave-one-out cross validation and plotted against the feature *defect area*. Diagnostic charts with a large defect area have higher prognostic accuracy than charts with only few defect areas.

and the respective rates of correctly labeled positive samples (TPR) and incorrectly labeled negative samples (FPR) were used to determine points in the ROC space [36] forming a continuous curve (see Fig. 7, top panel). For computation of the score, we propose a simple measure, which is based on the distance between the sample and the respective nearest map unit with a positive class (d_{hot}) and the nearest map unit with a negative class (d_{cold}). The score of the ith sample is then the relative distance

$$\mathrm{score}_i = \frac{d_{\mathrm{cold}}}{d_{\mathrm{hot}} + d_{\mathrm{cold}}} \tag{15}$$

which is a value between "0" (indicating that the ith sample is close to a map unit labeled "cold spot") and "1" (close to a "hot spot" map unit). With the features extracted as before, the performance of the SOM approach was compared with two other classifiers (see Fig. 7, top panel). First, the support vector machine (SVM) [42], with a 2-D polynomial kernel, showed comparable results, which were slightly better (AUC $= 0.83$, ACC $= 86.8 \pm 1.1\%$, TPR $= 45.3 \pm 4.5\%$, FPR $= 3.2 \pm 0.8\%$). Second, a 5-nearest neighbor classifier, based on the four principal components from a principal component analysis (PCA) with varimax rotation, showed the best results (AUC $= 0.92$, ACC $= 90.0 \pm 0.8\%$, TPR $= 68.5 \pm 4.0\%$, FPR $= 4.7 \pm 1.0\%$).

E. Clinical Evaluation

The appropriateness of the TOPM to several subclasses of patients is of clinical relevance. By separating the samples with respect to patient affiliation, leave-one-out cross validation showed that the performance is not equal for each subject, resulting in a high range of individual performance measures (minimal accuracy $= 29\%$, maximal accuracy $= 98\%$). A strong correlation between accuracy and the feature *Defect Area* ($\rho = 0.67$) shows (see Fig. 7, bottom panel) that the accuracy of diagnostic charts, with many defect areas, was better than in charts with only few defect areas.

IV. Discussion

When prediction models are used in the medical field, care must be taken because, unlike other classification problems (e.g., in the financial domain), the misclassification of patients could lead to changes in patient's treatment regimen. Patients could face serious consequences such as emotional stress (healthy subjects are misclassified, wrong promises, etc.), inappropriate treatment, or no treatment at all [41]. It has been suggested that such an analysis should go beyond the evaluation of statistical measures, such as the area under the ROC curve. Therefore, additional evaluations are necessary to assure clinical usefulness of a TOPM in general [17].

In the case of VRT, misclassification of treatment areas could result in longer treatment time or reduced treatment efficiency. There are some guiding principles that should be observed in assessing the clinical credibility, effectiveness, and evidence of generality and accuracy of prediction models in medicine [33]. TOPMs should not rely completely on correlation analysis of features and the treatment outcome [43]. To extend the correlation analysis, we have also used statistical tests to clarify that the differences between means of features in relation to cold and hot spots are statistically significant in order to ascertain that the feature is able to sufficiently separate the set of cold from the set of hot spots. Domain experts are needed to verify the appropriateness of the proposed classification principles using patient samples [44], which was fulfilled in the present study because VRT-domain experts utilized accepted standards in VRT research [47]. By close examination of the SOM units, which determine the class label in prediction, it is possible to analyze the rules on which the classification is determined, as required elsewhere [43]. Furthermore, it is recommended to use *a priori* knowledge such that the robustness of the prediction model is enhanced [21]. In this regard, we have used physiological knowledge of visual cortex organization and reorganization, visual cortex anatomy, and the experience of domain experts to construct appropriate features. Furthermore, the association between features and treatment outcome should be assessed in more than one population in order to reduce the risk of spurious associations between feature and class information [45]. In this regard, the feature extraction phase in the present study was based on two independent studies done within the last ten

years. Further work is required to confirm the clinical benefits of the developed TOPM for VRT because our results need to be replicated, confirmed, and further documented [43]. This requires rigorous testing, ideally in a double-blind, randomized, and placebo-controlled investigation [21].

We have chosen the SOM as core of the prediction model. Its nonlinearity and self-organization methodology allows a comprehensible adaptation to the data distribution. Although other prediction models may perform better, SOMs simplify the process of data mining and the feature selection phase by conveniently combining both prediction and data exploration.

V. Conclusion

We have presented a TOPM that allows prediction of restoration of vision and plasticity of impaired or blind topographic areas in the visual field of patients with visual system damage. The TOPM included features that are associated with the treatment outcome, as assessed by prior studies and described in the literature of VRT. The features incorporate *a priori* knowledge and address several topics in the broad field of vision recovery. This paper has shown how the SOM is useful for hypothesis selection when conducting research on perimetric visual field assessment. Furthermore, our study showed that the classification performance is robust and appropriate in predicting areas of greatest recovery potential in clinical settings. It is our hope that future studies will compare the results of the most relevant features of our model using multiple clinical parameters. This will be useful not only for further validation of the TOPM, but also for yielding new insights into mechanisms of vision restoration and the design of more effective treatment methods.

Acknowledgment

The authors would like to thank Dr. C. Borgelt for discussing SOMs, Dr. K. Haylett for the lively discussion about prediction models in medicine, and I. Pasley for her help preparing the paper. T. Guenther, M. Preuss, I. Mueller, and R. Kruse have no financial interest related to this paper. B. A. Sabel is shareholder of NovaVision, Inc.

References

[1] P. Sajda, "Machine learning for detection and diagnosis of disease," *Annu. Rev. Biomed. Eng.*, vol. 8, pp. 537–565, 2006.

[2] E. Kasten, S. Wuest, W. Behrens-Baumann, and B. A. Sabel, "Computer-based training for the treatment of partial blindness," *Nature Med.*, vol. 4, pp. 1083–1087, 1998.

[3] E. Kasten, D. A. Poggel, and B. A. Sabel, "Computer-based training of stimulus detection improves color and simple pattern recognition in the defective field of hemianopic subjects," *J. Cogn. Neurosci.*, vol. 12, pp. 1001–1012, 2000.

[4] I. Mueller, D. A. Poggel, S. Kenkel, E. Kasten, and B. A. Sabel, "Vision restoration therapy after brain damage: Subjective improvements of activities of daily life and their relationship to visual field enlargements," *Vis. Impairment Res.*, vol. 5, pp. 157–178, 2003.

[5] B. A. Sabel and E. Kasten, "Restoration of vision by training of residual functions," *Curr. Opin. Ophthalmol.*, vol. 11, pp. 430–436, 2000.

[6] L. M. Chalupa and J. S. Werner, *The Visual Neurosciences*. Bradford, U.K.: Bradford Book, 2004.

[7] D. Van Essen, "Organization of visual areas in macaque and human cerebral cortex," in *The Visual Neurosciences,* vol. 1, L. M. Chalupa and J. S. Werner, Eds. Cambdrige, MA: MIT Press, 2004, pp. 507–521.

[8] J. J. Barton and M. Benatar, *Field of Vision: A Manual and Atlas of Perimetry*. Totowa, NJ: Humana Press, 2003.

[9] P. G. Spry, C. A. Johnson, A. M. McKendrick, and A. Turpin, "Variability components of standard automated perimetry and frequency-doubling technology perimetry," *Invest. Ophthalmol. Vis. Sci.*, vol. 42, pp. 1404–1410, 2001.

[10] T. Guenther, J. Gudlin, B. A. Sabel, and I. Mueller, "Data infrastructure of prediction models for the diagnosis and treatment outcome in patients with visual system dysfunction," presented at the 3rd Int. Conf. Comput. Intell. Med. Healthc., Plymouth, U.K., Jul. 25–27, 2007.

[11] E. Kasten, H. Strasburger, and B. A. Sabel, "Programs for diagnosis and therapy of visual field deficits in vision rehabilitation," *Spat. Vis.*, vol. 10, pp. 499–503, 1997.

[12] Y. M. Chino, E. L. Smith,III, J. H. Kaas, Y. Sasaki, and H. Cheng, "Receptive-field properties of deafferentated visual cortical neurons after topographic map reorganization in adult cats," *J. Neurosci.*, vol. 15, pp. 2417–2433, 1995.

[13] S. J. Sober, J. M. Stark, D. S. Yamasaki, and W. W. Lytton, "Receptive field changes after strokelike cortical ablation: A role for activation dynamics," *J. Neurophysiol.*, vol. 78, pp. 1–6, 1997.

[14] S. J. Heinen and A. A. Skavenski, "Recovery of visual responses in foveal V1 neurons following bilateral foveal lesions in adult monkey," *Exp. Brain Res.*, vol. 83, pp. 670–674, 1991.

[15] E. Kasten, D. A. Poggel, E. Müller-Oehring, J. Gothe, T. Schulte, and B. A. Sabel, "Restoration of vision II: Residual functions and training-induced visual field enlargement in brain-damaged patients," *Restor. Neurol. Neurosci.*, vol. 15, pp. 273–287, 1999.

[16] B. Sabel, S. Kenkel, and E. Kasten, "Vision restoration therapy (VRT) efficacy as assessed by comparative perimetric analysis and subjective questionnaires," *Restor. Neurol. Neurosci.*, vol. 22, pp. 399–420, 2004.

[17] A. Abu-Hanna and P. J. F. Lucas, "Editorial: Prognostic models in medicine," *Methods Inf. Med.*, vol. 40, pp. 1–5, 2001.

[18] H. Mast, M. Preuss, and B. A. Sabel, "Vision restoration therapy vs. exploration training in patients with visual field loss," presented at the Neural Plast. Neurorehabil., Zurich, Switzerland, Jun. 26–30, 2006.

[19] F. A. Ubaudi, "Development of a treatment outcome prediction model for childhood leukaemia," Dissertation, Bioinform. Res. Centre, Univ. Technol., Sydney, N.S.W., Australia, 2005.

[20] E. Alexopoulos, G. Dounias, and K. Vemmos, "Medical diagnosis of stroke using inductive machine learning," in *Proc. Workshop Mach. Learn. Med. Appl., Adv. Course Artif. Intell.*, Chania, Greece, Jul. 5–16, 1999, pp. 20–23.

[21] P. J. Lucas and A. Abu-Hanna, "Prognostic methods in medicine," *Artif. Intell. Med.*, vol. 15, pp. 105–119, 1999.

[22] T. Guenther, "Data mining in diagnostic charts and treatment outcome prediction for vision restoration therapy," Ph.D. dissertation, Otto-von-Guericke Univ., Magdeburg, Germany, 2008.

[23] E. Kasten and B. A. Sabel, "Visual field enlargement after computer training in brain-damaged patients with homonymous deficits: An open pilot trial," *Restor. Neurol. Neurosci.*, vol. 8, pp. 113–127, 1995.

[24] D. A. Poggel, I. Mueller, E. Kasten, and B. A. Sabel, "Multifactorial predictors and outcome variables of vision restoration therapy in patients with visual field loss," *Restor. Neurol. Neurosci.*, vol. 26, pp. 321–339, 2008.

[25] D. A. Poggel, E. Kasten, and B. A. Sabel, "Attentional cueing improves vision restoration therapy in patients with visual field defects," *Neurology*, vol. 63, pp. 2069–2076, 2004.

[26] I. Mueller, D. A. Poggel, E. Kasten, and B. A. Sabel, "Predicting the outcome of visual restitution training: A retrospective clinical study on visual system plasticity," presented at the 30th Annu. Meeting Soc. Neurosci., Orlando, FL, Nov. 2–7, 2002.

[27] D. A. Poggel, E. Kasten, E. M. Muller-Oehring, U. Bunzenthal, and B. A. Sabel, "Improving residual vision by attentional cueing in patients with brain lesions," *Brain Res.*, vol. 1097, pp. 142–148, 2006.

[28] D. A. Poggel, "Effects of visuo-spatial attention on the restitution of visual field defects in patients with cerebral lesions," Ph.D. dissertation, Otto-von-Guericke Univ., Magdeburg, Germany, 2002.

[29] E. Kasten, S. Wuest, and B. A. Sabel, "Residual vision in transition zones in patients with cerebral blindness," *J. Clin. Exp. Neuropsychol.*, vol. 20, pp. 581–598, 1998.

[30] B. A. Sabel, "Editorial: Residual vision and plasticity after visual system damage," *Restor. Neurol. Neurosci.*, vol. 15, pp. 73–79, 1999.

[31] T. Guenther, M. Preuss, and I. Mueller, "Coordinate-transformation module connecting the visual cortex and the visual space," presented at the Int. Conf. Artif. Intell. Pattern Recognit., Orlando, FL, Jul. 9–12, 2007.

[32] T. Kohonen, "The self-organizing map," *Proc. IEEE*, vol. 78, no. 9, pp. 1464–1480, Sep. 1990.
[33] J. C. Wyatt and D. G. Altman, "Commentary: Prognostic models: Clinically useful or quickly forgotten?," *Br. Med. J.*, vol. 311, no. 7019, pp. 1539–1541, 1995.
[34] J. Vesanto, "SOM-based data visualization methods," *Intell. Data Anal.*, vol. 3, pp. 111–126, 1999.
[35] K. Veropoulos, "Machine learning approaches to medical decision making," Dissertation, Univ. Bristol, Bristol, U.K., 2001.
[36] T. Fawcett, "ROC graphs: Notes and practical considerations for researchers," HP Lab., Palo Alto, CA, Tech. Rep., Apr. 2004.
[37] M. Green and M. Ohlsson, "Comparison of standard resampling methods for performance estimation of artificial neural network ensembles," presented at the 3rd Int. Conf. Comput. Intell. Med. Healthcare, Plymouth, U.K., Jul. 25–27, 2007.
[38] W. J. Youden, "Index for rating diagnostic tests," *Cancer*, vol. 3, pp. 32–35, 1950.
[39] R. C. Holte, "Very simple classification rules perform well on most commonly used datasets," *Mach. Learn.*, vol. 11, no. 1, pp. 63–90, Apr. 1993.
[40] J. A. Swets and R. M. Pickett, *Evaluations of Diagnostic Systems: Methods From Signal Detection Theory*. New York: Academic, 1982.
[41] M. S. Pepe, "Evaluating technologies for classification and prediction in medicine," *Stat. Med.*, vol. 24, pp. 3687–3696, 2005.
[42] C.-C. Chang and C.-J. Lin, *LIBSVM: A Library for Support Vector Machines*, 2001.
[43] A. Shillabeer and J. F. Roddick, "On the arguments against the application of data mining to medical data analysis," presented at the Intell. Data Anal. BioMed. Pharmacol., Verona, Italy, 2006.
[44] R. Ruseckaite, "Computer interactive system for ascertainment of visual perception disorders," in *Proc. Workshop Mach. Learn. Med. Appl., Adv. Course Artif. Intell.*, Chania, Greece, Jul. 5–16, 1999, pp. 27–29.
[45] G. D. Smith and S. Ebrahim, "Data dredging, bias, or confounding," *BMJ*, vol. 325, pp. 1437–1438, 2002.
[46] D. D. Stettler, A. Das, J. Bennett, and C. D. Gilbert, "Lateral connectivity and contextual interactions in macaque primary visual cortex," *Neuron*, vol. 36, pp. 739–750, 2002.
[47] I. Mueller, H. Mast, and B. A. Sabel, "Recovery of visual field defects: A large clinical observational study using vision restoration therapy," *Restor. Neurol. Neurosci.*, vol. 25, no. 5/6, pp. 563–572, 2007.

Tobias Guenther received the Diploma and the Dr.-Ing. degree in computer science from Otto-von-Guericke University, Magdeburg, Germany, in 2004 and 2008, respectively.

During 2002 and 2004, he was with the Fraunhofer Institute of Autonomous Intelligent Systems, Sankt Augustin, Germany. He joined the Institute of Medical Psychology, Otto-von-Guericke University. His current research interests include computer vision, data mining, and human visual perception. He founded Elaspix UG, Mannheim, Germany, where he is currently involved in image processing tools.

Mr. Guenther has been a referee in the First Lego League and the Robocup Junior Dance competition since 2005.

Iris Mueller received the Diploma in psychology from the Technical University of Braunschweig, Braunschweig, Germany, in 1998, and the Doctoral degree from Otto-von-Guericke University, Magdeburg, Germany, in 2006.

She studied neuropsychology at the Clinic of Neurology, University of Innsbruck, Austria, and at the University of Minnesota, where she was with the Pediatric Neurology Department, and with the Pediatric Neuropsychology Unit for a one-year Internship Program. She was involved in the field of diagnostic and therapy outcome of patients with autism, attentional disorder, and visual impairment after congenital and acquired brain injury. In 2000, she joined the Institute of Medical Psychology, Otto-von-Guericke University, where she was engaged in the treatment outcome prediction of cerebral caused visual perception impairments in children as well as in adults. In 2003, she became the Team Lead of the group "Theoretical Neuropsychology," which focuses on research of clinical mechanisms of visual learning after brain lesions.

Markus Preuss received the Diploma in psychology from the Rheinische Friedrich-Wilhelms-University of Bonn, Bonn, Germany, in 2003.

From 2004 to 2007, he was a Researcher and a Lecturer at the Institute of Medical Psychology, Otto-von-Guericke-University of Magdeburg, Magdeburg, Germany, and at the Institute for Medical Information Processing, Biometry and Epidemiology, Ludwig-Maximilians-University, Munich, Germany. Since 2008, he has been a Scientist at the Institute of Preventive Medicine, University of Rostock, Rostock, Germany, where he is also a Researcher at the Center for Life Science Automation, Warnemünde. His current research interests include neuropsychology, occupational psychology, and the modeling of emotions based on secondary physiological data. With his prediction model of usability-related emotions, he is engaged in improvement of human–machine interfaces.

Rudolf Kruse (M'94–SM'95–F'05) received the Diploma and the Ph.D. and venia legendi degrees from the University of Braunschweig, Braunschweig, Germany, in 1979, 1980, and 1984, respectively, all in mathematics.

He was at the Fraunhofer Gesellschaft. In 1986, he joined the University of Braunschweig as a Professor of computer science. Since 1996, he has been a Full Professor in the Department of Computer Science, Otto-von-Guericke University, Magdeburg, Germany, where he is leading the Computational Intelligence Research Group. He was engaged in research and projects in statistics, artificial intelligence, expert systems, fuzzy control, fuzzy data analysis, computational intelligence, and data mining. He has authored or coauthored 12 monographs, 15 edited books as well as more than 300 refereed technical papers in various scientific areas. He is an Associate Editor of several scientific journals.

Prof. Kruse is a Fellow of the International Fuzzy Systems Association (IFSA) and the European Coordinating Committee for Artificial Intelligence (ECCAI).

Bernhard A. Sabel received the M.A. degree in psychology from the University of Düsseldorf, Düsseldorf, Germany, in 1982, and the Ph.D. degree in psychobiology from Clark University, Worcester, MA, in 1984.

He was a Postdoctoral Fellow at the Massachusetts Institute of Technology (M.I.T.), Cambridge, and a Research Scientist at the University of Munich, Munich, Germany from 1987 to 1992. During 1991, he was a Visiting Neuroscientist at the Massachusetts General Hospital, Department of Neurology, Harvard Medical School. During 1998 and 1999, he was a Research Fellow in the Department of Psychology, Princeton University. Since 1992, he has been the Director of the Institute of Medical Psychology, Medical Faculty, Otto-von-Guericke University, Magdeburg, Germany, where he has also been the University Vice President for Research and Technology Transfer since 2008. His current research interests include brain plasticity and recovery of function following brain damage in animals and patients, with a focus on vision restoration therapy (VRT), a training software for patients with visual field deficits, electrical brain synchronization technology for rehabilitation, and nanoparticle technology for drug delivery and drug targeting to the brain.

Dr. Sabel has been Governor of the International Brain Injury Association (IBIA) since 2008. He is the Editor-in-Chief of the *Restorative Neurology and Neuroscience* (1997).